



Figures and figure supplements

An arbitrary-spectrum spatial visual stimulator for vision research

Katrin Franke et al

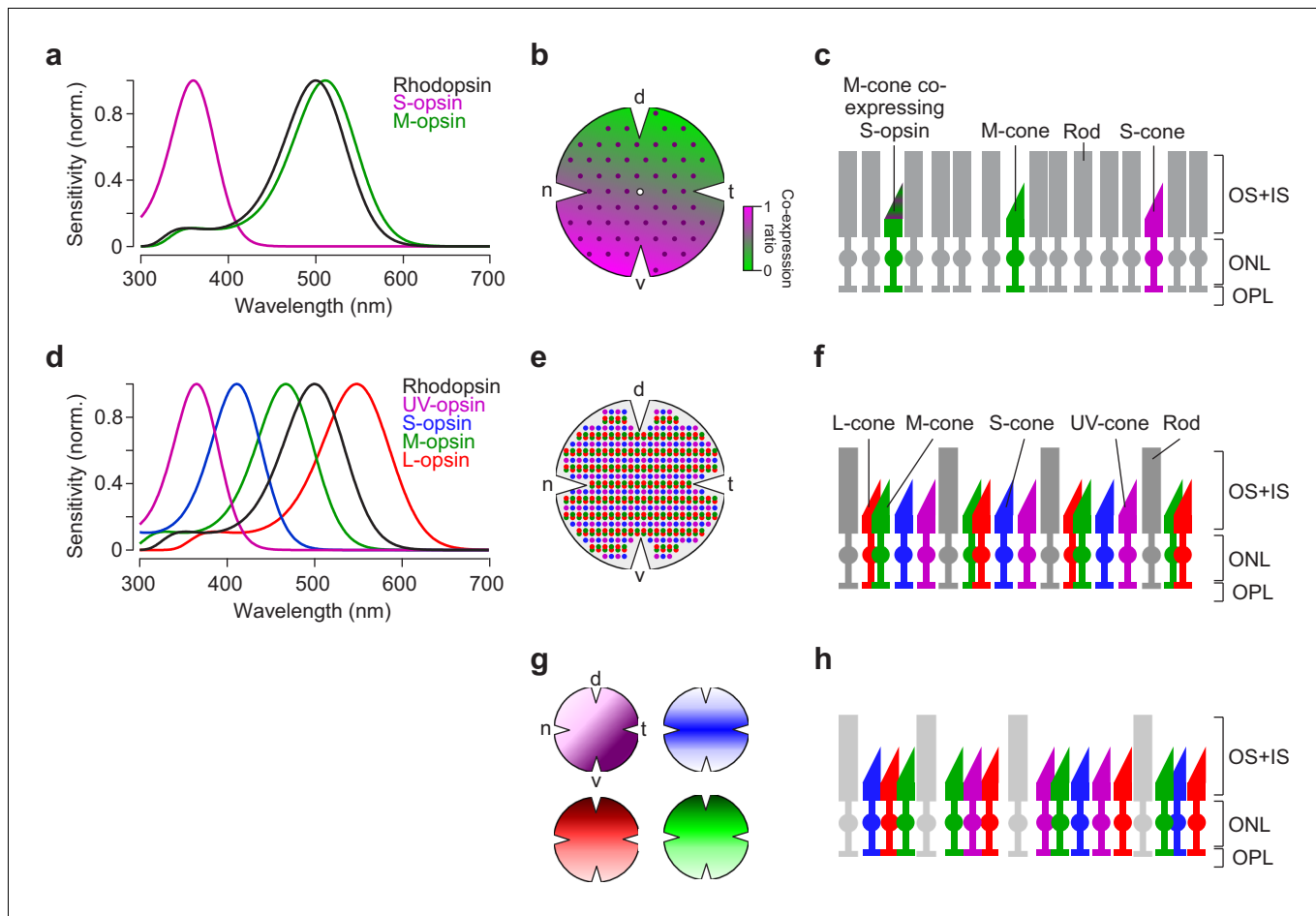


Figure 1. Photoreceptor types and distribution in mouse and zebrafish retina. (a) Peak-normalised sensitivity profiles of mouse S- (magenta) and M-opsin (green) as well as rhodopsin (black; profiles were estimated following **Stockman and Sharpe, 2000**). (b) Schematic drawing of the distribution of cone photoreceptor (cone) types in the mouse; rod photoreceptors (rods) are homogeneously distributed (**Jeon et al., 1998**) (not shown here). Purple dots represent 'true' S-cones exclusively expressing S-opsin (**Haverkamp et al., 2005**); ratio of co-expression of S-opsin in M-cones (**Applebury et al., 2000; Baden et al., 2013**) is colour-coded from green to magenta (d, dorsal; t, temporal; v, ventral; n, nasal). (c) Illustration of mouse cone and rod arrangement (vertical view; OS+IS, outer and inner segments; ONL, outer nuclear layer; OPL, outer plexiform layer). (d) Peak-normalised sensitivity profiles of zebrafish UV- (magenta), S- (blue), M- (green) and L-opsin (red) as well as rhodopsin (black). (e) Schematic illustration of the regular cone arrangement in adult zebrafish. Coloured dots represent UV-, S-, M- and L-cones. (f) Like (c) but for adult zebrafish retina. (g) Schematic drawing illustrating the distribution of cone types in zebrafish larvae (**Zimmermann et al., 2018**). Colours as in (d). (h) Like (c,f) for zebrafish larvae. Lighter colour of rods indicate that they are not functional at this age (7–9 dpf; **Branchek and Bremiller, 1984; Morris and Fadool, 2005**).

DOI: <https://doi.org/10.7554/eLife.48779.002>

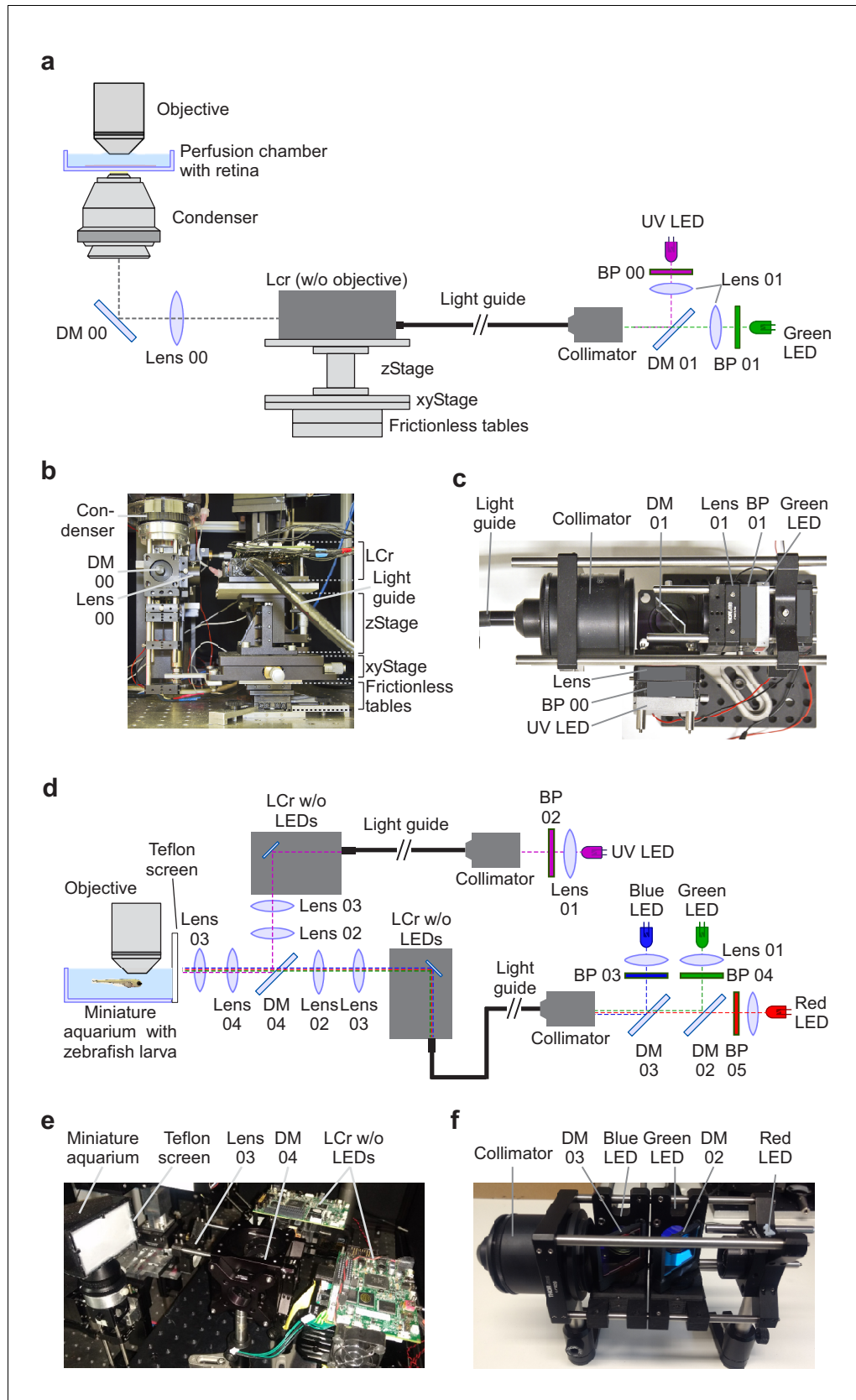


Figure 2. Visual stimulator design. (a) Schematic drawing of the dichromatic stimulator for in vitro recordings of mouse retinal explants. The stimulator is coupled into the two-photon (2P) microscope from below the recording. Figure 2 continued on next page

Figure 2 continued

chamber with the retinal tissue (through-the-condenser; for alternative light paths (through-the-objective), see **Figure 2—figure supplement 1**). DM, dichroic mirror; BP, band-pass filter; LCr, lightcrafter; LED, light-emitting diode. For components, including custom-made parts, see **Table 2**. (b) LCr unit and substage portion of the 2P microscope in side-view. (c) External LED illumination unit in top-view. For details on mechanical parts, see **Figure 2—figure supplement 6**. (d) Schematic drawing of the tetrachromatic stimulator for *in vivo* recordings in zebrafish larvae. The optical pathways of two LCrs are combined and the stimulus is projected onto a UV-transmissive teflon screen at one side of the miniature aquarium. For components, see **Table 3**. (e) Side-view of tetrachromatic stimulation setup. (f) RGB external LED illumination unit of tetrachromatic stimulation setup. Band-pass (BP) filters 03, 04 and 05 as well as lenses 01 are not indicated due to space constraints.

DOI: <https://doi.org/10.7554/eLife.48779.004>

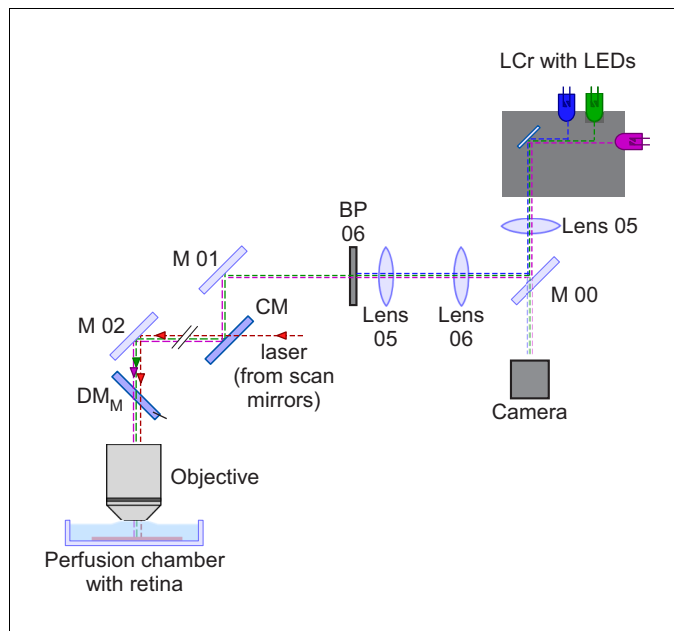


Figure 2—figure supplement 1. Optical pathway for a through-the-objective (TTO) mouse stimulator. Schematic drawing of a TTO dichromatic stimulator for in vitro recordings of mouse retinal explants (cf. Euler et al., 2009). The light from the LCr with internal UV, blue and green LEDs is filtered by a dual-band filter transmitting UV and green light. Then, the light is coupled into the two-photon microscope using a cold mirror (CM). Using a beam-splitter (M 00), a small fraction of light is projected onto a camera to allow online visualisation of the visual stimulus. LCr, lightcrafter; LED, light-emitting diode; M, mirror; CM, cold mirror; DM_M, dichroic mirror mouse; BP, band-pass filter. For specifications of the components, see **Table 2** and **Supplementary file 1**.

DOI: <https://doi.org/10.7554/eLife.48779.005>

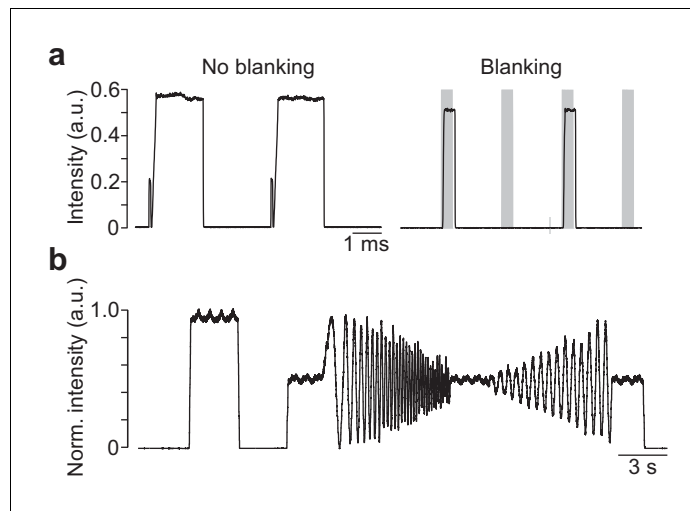


Figure 2—figure supplement 2. Intensity measurements of the LEDs of the mouse stimulator. (a) Intensity of green LED measured with a PMT (at 250 kHz; for details, see Materials and methods) without (left) and with blanking (right); grey shading indicates blanking signal. (b) Smoothed (box smooth, box width: 100 ms) intensity profile of a full-field chirp stimulus recorded with a fast photodiode.

DOI: <https://doi.org/10.7554/eLife.48779.006>

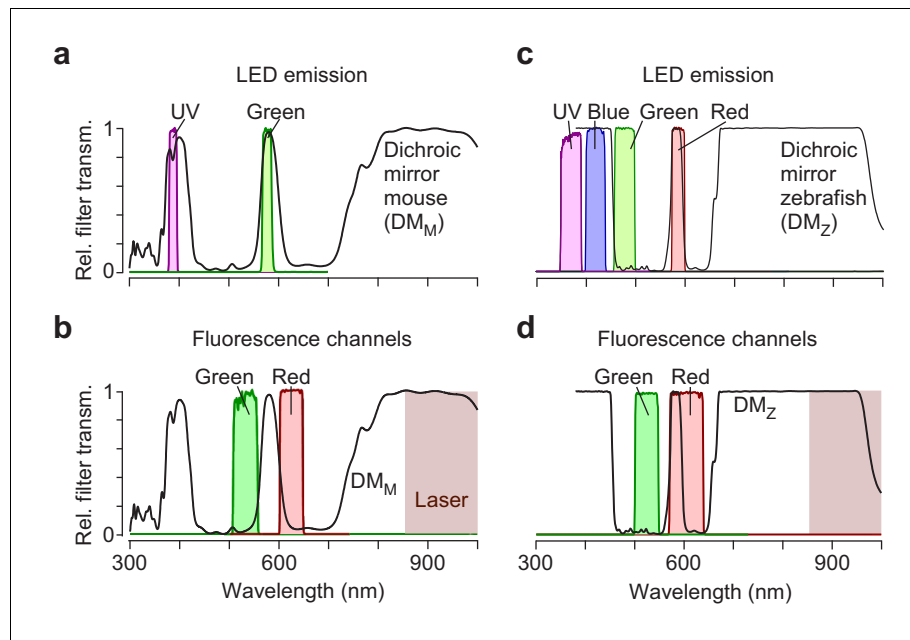


Figure 2—figure supplement 3. Spectral separation of visual stimulation and fluorescence detection. (a) Relative transmission of filters in front of UV and green LED as well as of dichroic mirror on top of objective (cf. Euler et al., 2009). (b) Same as (a), for filters in front of PMTs (Materials and methods). Burgundy shading illustrates the wavelength range used for two-photon laser. (c, d) Like (a) and (b) but for zebrafish stimulator.

DOI: <https://doi.org/10.7554/eLife.48779.007>

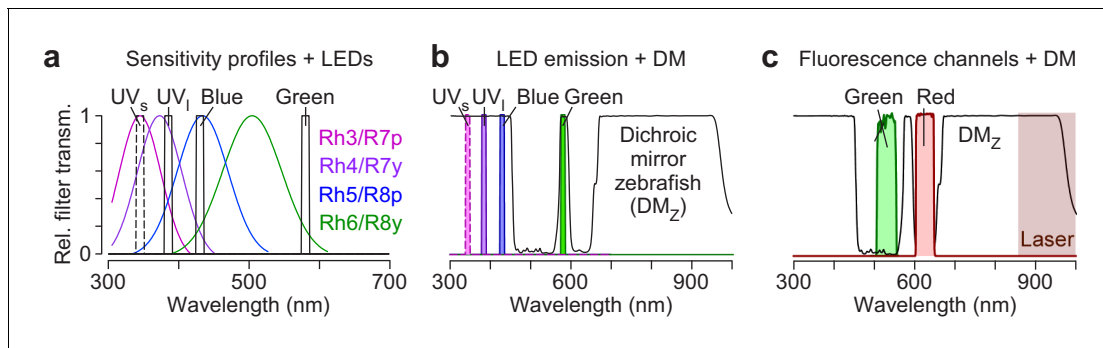


Figure 2—figure supplement 4. Suggestion for LED/filter design for a *Drosophila* visual stimulator. (a) Spectral sensitivity of rhodopsins expressed in the four types of inner photoreceptors (Rh3: short-UV; Rh4: long-UV; Rh5: blue; Rh6: green) of *Drosophila* (data from **Schnaitmann et al., 2018**, based on **Salcedo et al., 1999**), with a possible combination of band pass-filtered LEDs for chromatic stimulation (black). Dotted line for the short-UV LED indicates that for wavelengths < 380 nm, additional optimisation of the optical parts within the LCr is required (see Discussion). (b) Suggested filter combination (black) from (a) can be combined with the dichroic mirror used for the zebrafish stimulator (DM_Z; grey). (c) DM_Z with suitable filters in front of PMTs for detection of green (535/50 BrightLine HC, AHF) and red (630/38 BrightLine HC, AHF) fluorescence. Burgundy shading marks wavelength range used for 2P laser.

DOI: <https://doi.org/10.7554/eLife.48779.008>

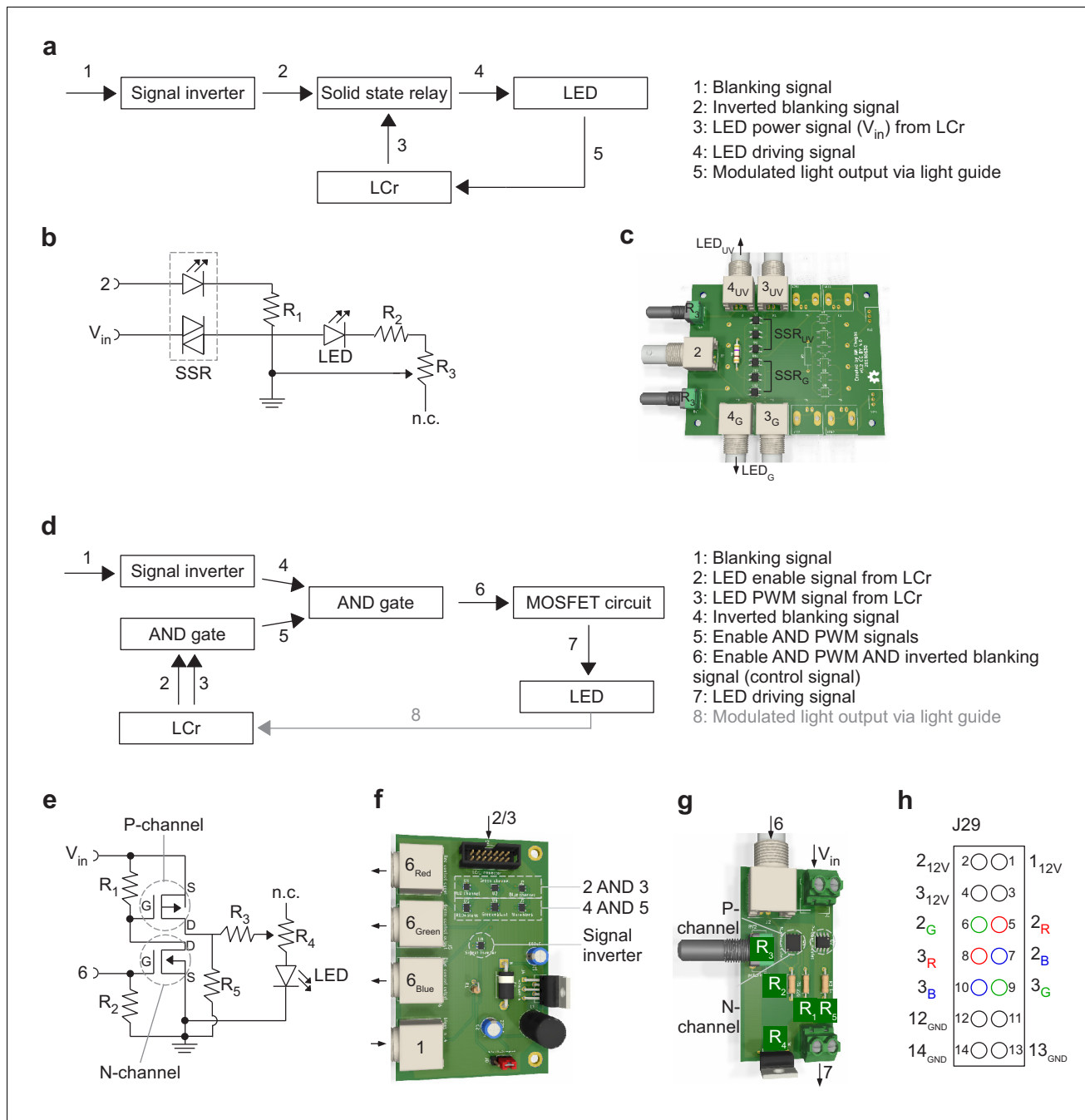


Figure 2—figure supplement 5. External LED control and temporal separation of stimulation and fluorescence detection. (a) Schematic illustrating the circuit that ensures that the stimulator LEDs are only on during the microscope's scanner retrace (for details, see Results). The 'laser blanking' signal (1) generated by the scan software is inverted (2) and then used to drive solid-state relays that modulate the LED power signal generated by the LCr (3). This modulated power signal (4) drives the LEDs. The LED light (5) is fed to the LCr via a light guide. (b) Wiring diagram of the solid-state relay (SSR) circuit (signals like in (a); $R_1 = 220 \Omega$, the values for R_2 and potentiometer R_3 depend on the LEDs used and typically are in the range of 0–500 Ω). (c) Rendering of the custom-printed circuit board, which can accommodate up to four LED channels (only the components for two channels are soldered). (d) Schematic illustrating an alternative circuit to (a–c), where the LEDs are powered from an external supply. Here, the LCr LED control signals (2, 3) go through a logical AND operation and the resulting signal (5) is then combined with the inverted blanking signal (4). The resulting signal (6) is used to switch the LED power using a combination of P and N-channel MOSFETs (cf. (e)). Finally, the LED power signal (7) drives the internal or external LEDs. (e) Wiring diagram of the MOSFET circuit (signals as in (d); $R_1 = 220 \Omega$, $R_2 = 220 \Omega$, $R_3 = 0.5 \Omega$, potentiometer $R_4 = 25 \Omega$, $R_5 = 1 k\Omega$). (f,g) Rendering of two custom-printed boards responsible for combining the control signals (logic board), up to three LED channels per board (f) and switching the LEDs (driver board), just one LED channel per board (g). (h) Pinout of connector J29 ('external LED driver connector') on the LCr board. To disable the LCr's

Figure 2—figure supplement 5 continued on next page

Figure 2—figure supplement 5 continued

internal LED drivers, jumper J30 must be installed, while J28 is used to choose between 3.3V or 1.8V supply voltage (see **Table 1** for links to LCr instruction manuals).

DOI: <https://doi.org/10.7554/eLife.48779.009>

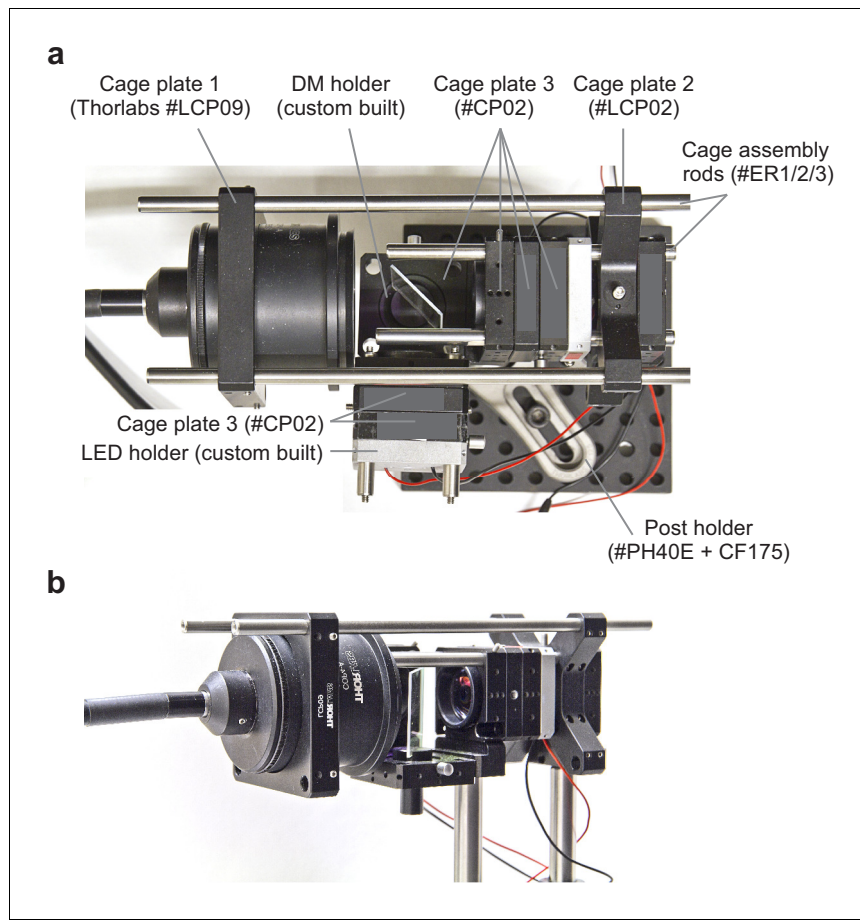


Figure 2—figure supplement 6. Detailed description of external LED unit of the mouse stimulator. (a) Top-view of external LED illumination unit, with ordering numbers of all parts purchased from Thorlabs indicated (see also **Table 2**). Cage plates #LCP02 holds filters and lenses with a diameter of 0.5". DM (Nylon) and DM and LED holders (Aluminium) were custom-built by the University workshop (**Table 2**); the latter resemble Thorlab's cage plates but with mounting holes for the LEDs. The LED holders dissipate the heat from the relatively low-power LEDs used for the mouse and zebrafish stimulator sufficiently, such that a cooling fan was not needed. (b) Side-view of external LED illumination unit.

DOI: <https://doi.org/10.7554/eLife.48779.010>

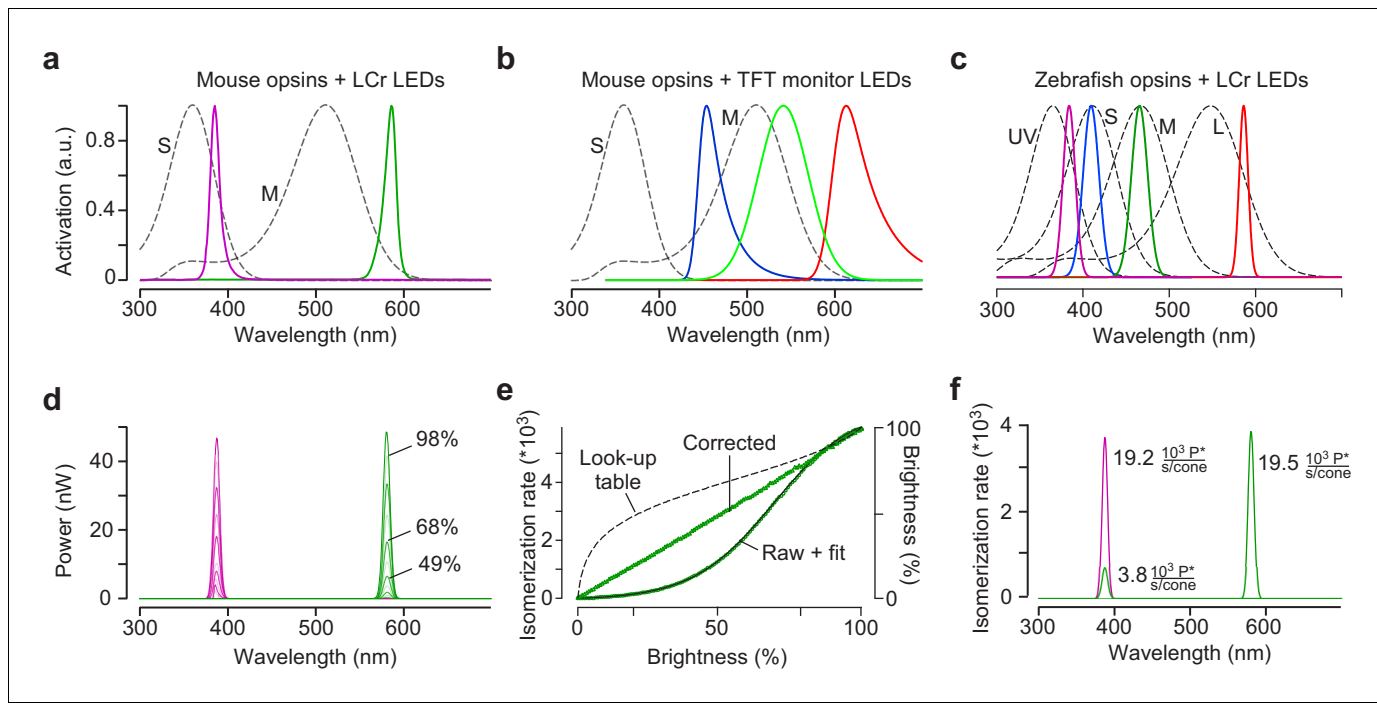


Figure 3. Calibration of the mouse stimulator. (a) Sensitivity profiles of mouse S- and M-opsin (dotted black lines) and spectra of UV (magenta) and green LED/filter combinations used in the mouse stimulator. (b) Sensitivity profiles of mouse S- and M-opsin (dotted black line) and spectra of blue, green and red LED present in a standard TFT monitor. (c) Sensitivity profiles of zebrafish opsins (dotted black lines) and spectra of UV, blue, green and red LEDs used in the zebrafish stimulator. (d) Spectra (in nW) of UV and green LED obtained from measurements using increasing brightness levels; shown are spectra for 0, 9, 19, 29, 39, 49, 59, 68, 78, 88, and 98% brightness. (e) Non-linearised intensity curve ('raw') with sigmoidal fit (black), estimated gamma correction curve (black dotted line; 'Look-up table') and linearized intensity curve ('corrected') for green LED. (f) Photoisomerisation rates for maximal brightness of UV (19.2 and 3.8 $\times 10^3$ P*/second/cone for S- and M-opsin, respectively) and green LED (0 and 19.5 $\times 10^3$ P*/second/cone for S- and M-opsin, respectively). Note that the UV LED also activates M-opsin due to its increased sensitivity in the short wavelength range (β -band, Discussion).

DOI: <https://doi.org/10.7554/eLife.48779.013>

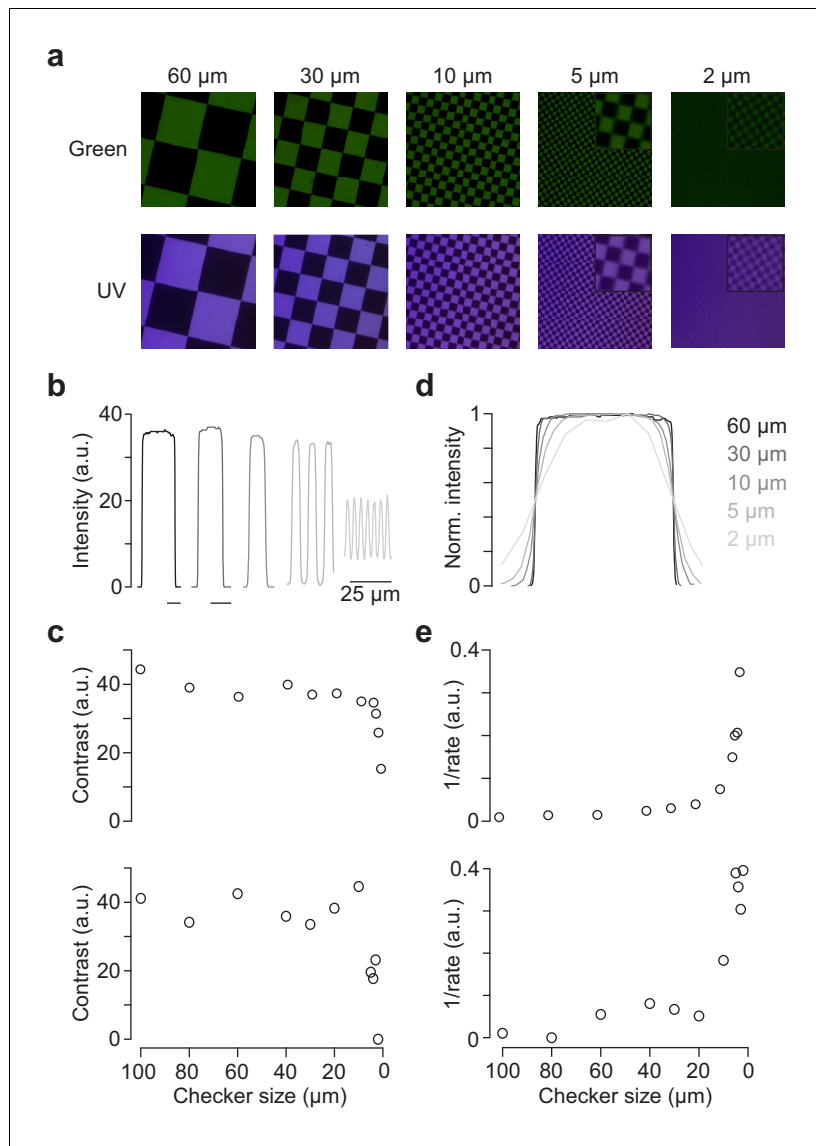


Figure 4. Spatial calibration of the mouse stimulator. (a) Images of checkerboard stimuli with varying checker sizes projected through-the-objective (TTO) for illumination with green (top) and UV (bottom) LED, recorded by placing the sensor chip of a Raspberry Pi camera at the level of the recording chamber. Focus was adjusted for UV and green LED separately. Insets for 5 and 2 μm show zoomed in regions of the image. (b) Intensity profiles for five different checker sizes of green LED. (c) Contrasts ($I_{\text{Max}} - I_{\text{Min}}$) for checkerboards of varying checker sizes of the TTO (top) and through-the-condenser (TTC; bottom) configuration. (d) Peak-normalised intensity profiles of different checker sizes, scaled to the same half-maximum width. (e) 1/rate estimated from sigmoidal fits of normalised intensity curves like in (d) for varying checker sizes of the TTO (top) and TTC (bottom) configuration.

DOI: <https://doi.org/10.7554/eLife.48779.014>

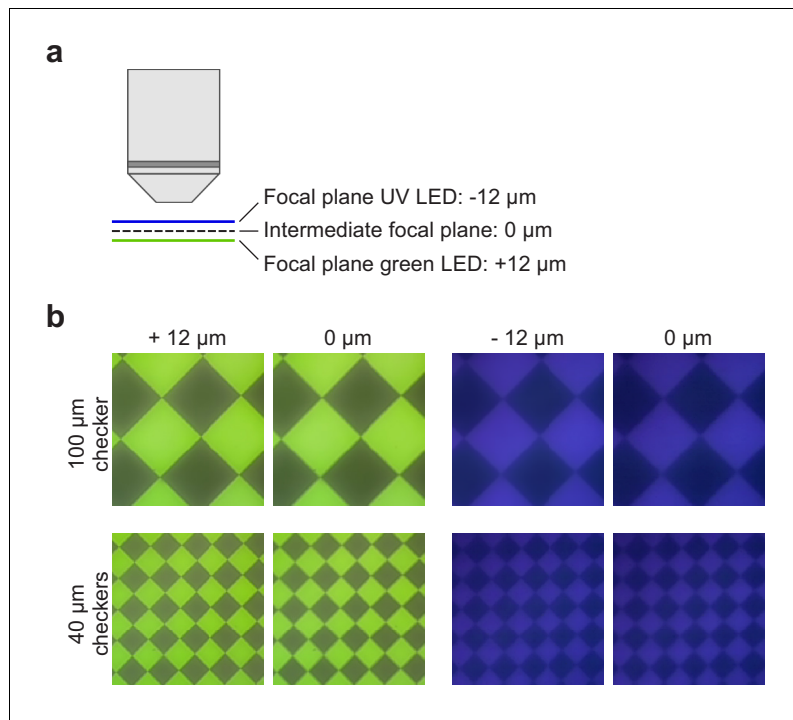


Figure 4—figure supplement 1. Chromatic aberration of the mouse stimulator. **(a)** Schematic illustrating the chromatic aberration-related difference in focal planes of UV and green image in the TTO configuration. **(b)** Images of a 100 (top) and 40 (bottom) μm checkerboard stimulus using the green (left) and UV (right) LED, recorded by placing the sensor chip of a Raspberry Pi camera at the level of the recording chamber. Focus was set to intermediate focal plane (see (a); $\pm 12 \mu\text{m}$) or was adjusted for UV and green LED separately (0 μm).

DOI: <https://doi.org/10.7554/eLife.48779.015>

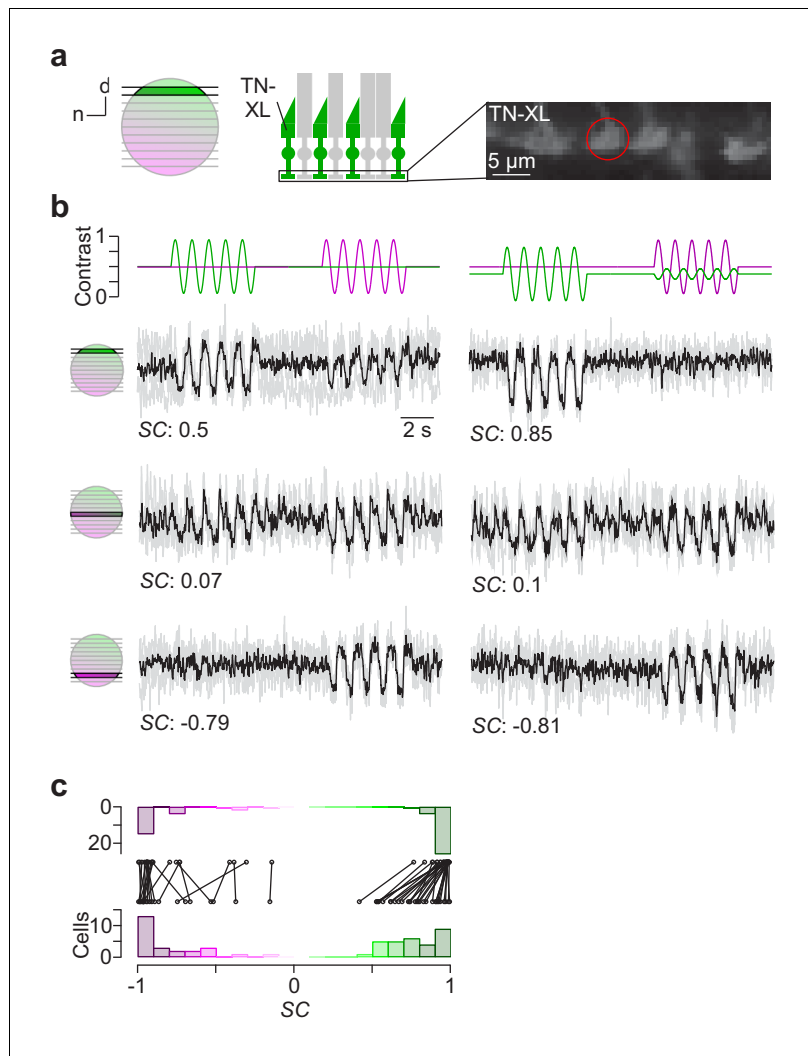


Figure 5. Cone-isolating stimulation of mouse cones. (a) Dorsal recording field in the outer plexiform layer (OPL; right) shows labelling of cone axon terminals with Ca^{2+} biosensor TN-XL in the HR2.1:TN-XL mouse line (Wei et al., 2012). Schematic on the left illustrates retinal location of recorded slice. (b) Ca^{2+} traces (mean traces in black, $n = 3$ trials in grey) of cone axon terminals located in dorsal (top; cone axon terminal from (a)), medial (middle) and ventral (bottom) retina in response to 1 Hz sine modulation of green and UV LED, with spectral contrast (SC) indicated below. Colour substitution protocol (right) estimated from calibration data (Materials and methods). (c) Distribution and comparison of SC for sine modulation stimulus with (top) and without (bottom) silent substitution protocol ($n = 55$ cells, $n = 12$ scan fields, $n = 1$ mouse; $p = 9.31 \times 10^{-9}$ for dorsal cells, $n = 30$; $p = 0.92$ for ventral cells, $n = 25$; Wilcoxon signed-rank test).

DOI: <https://doi.org/10.7554/eLife.48779.016>

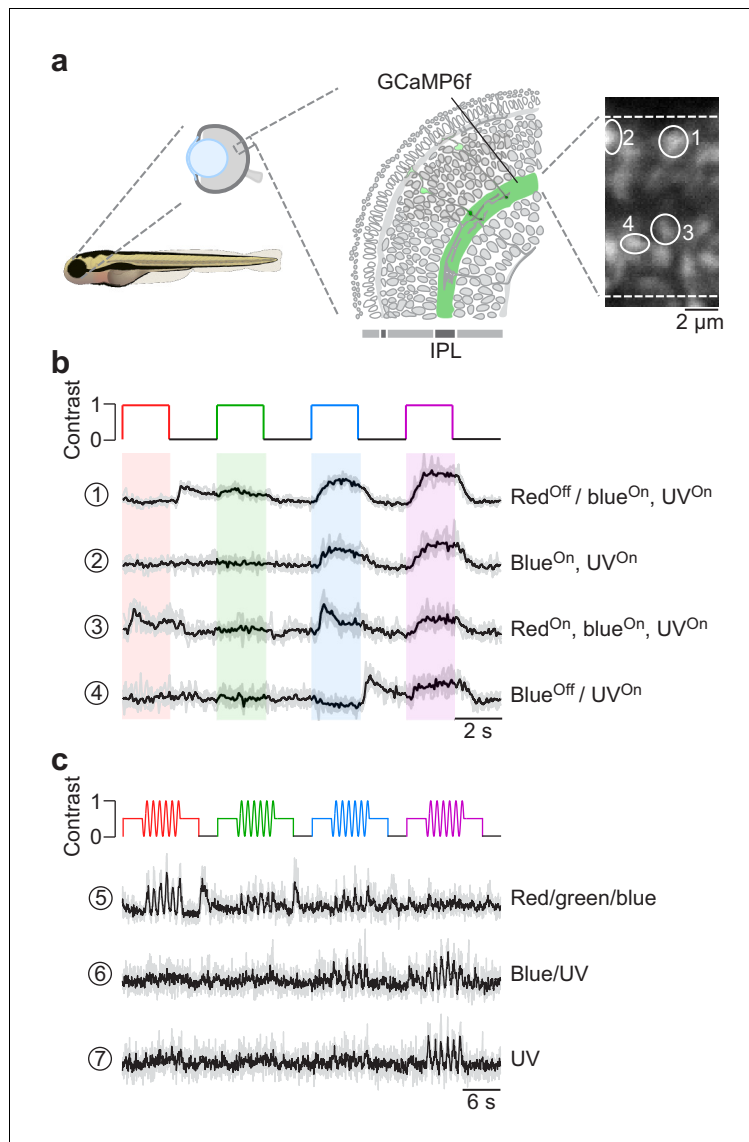


Figure 6. Chromatic responses in bipolar cells of in vivo zebrafish larvae. (a) Drawing illustrating the expression of the genetically encoded Ca^{2+} biosensor SyGCaMP6f in bipolar cell terminals (left) of *tg(1.8ctbp2:SyGCaMP6f)* zebrafish larvae and scan field of inner plexiform layer (IPL; right), with exemplary regions-of-interest (ROIs) marked by white circles. (b) Mean Ca^{2+} traces (black; $n = 6$ trials in grey) in response to red, green, blue and UV full-field flashes (90×120 degrees visual angle, presented to the fish's right side). (c) Mean Ca^{2+} traces (black; $n = 4$ trials in grey) in response to full-field sine modulation (at 1 Hz) of red, green, blue and UV LED.

DOI: <https://doi.org/10.7554/eLife.48779.017>